



**UNIVERSITI PUTRA MALAYSIA**

***ELECTRICAL PROPERTIES OF MIXED OXIDES OF MANGANESE AND  
VANADIUM PREPARED BY CONVENTIONAL SOLID STATE AND  
MECHANICAL ALLOYING METHODS***

**TAN FOO KHOON**

**ITMA 2016 11**



**ELECTRICAL PROPERTIES OF MIXED OXIDES OF MANGANESE AND  
VANADIUM PREPARED BY CONVENTIONAL SOLID STATE AND  
MECHANICAL ALLOYING METHODS**

**By**

**TAN FOO KHOON**

**Thesis Submitted to the School of Graduate Studies, Universiti Putra Malaysia, in  
Fulfillment of the Requirement of the Degree of Doctor of Philosophy**

**June 2016**



© COPYRIGHT UPM

All material contained within the thesis, including without limitation text, logos, icons, photographs and all other artwork, is copyright material of Universiti Putra Malaysia unless otherwise stated. Use may be made of any material contained within the thesis for non-commercial purposes from the copyright holder. Commercial use of material may only be made with the express, prior, written permission of Universiti Putra Malaysia.

Copyright © Universiti Putra Malaysia



## **SPECIALLY DEDICATED TO**

- My friendly and helpful supervisory committee, Assoc. Prof. Dr. Jumiah Hassan, the late Assoc. Prof. Mansor Hashim and Assoc. Prof. Zaidan Abdul Wahab.
- My beloved wife and family members for their moral support and encouragement.
- My seniors, lab mate and all my friends for their assistance.



Abstract of thesis presented to the Senate of Universiti Putra Malaysia in fulfilment of the requirement for the degree of Doctor of Philosophy

**ELECTRICAL PROPERTIES OF MIXED OXIDES OF MANGANESE AND VANADIUM PREPARED BY CONVENTIONAL SOLID STATE AND MECHANICAL ALLOYING METHODS**

By

**TAN FOO KHOON**

**June 2016**

**Chairman : Jumiah Hassan, PhD**  
**Faculty : Institute of Advanced Technology**

Metal oxide of manganese (Mn) and vanadium (V) are widely studied due to their interesting fundamental physical properties. There were several works on Mn-V mixed oxide done previously, but it still lacks comprehensive electrical studies on Mn-V oxide system which can give more information to describe the mixed oxide. In this project, the investigation toward morphology, electrical conductivity, dielectric properties and thermal diffusivity of the mixed oxides was carried out. The samples were prepared by conventional solid state (SS) and mechanical alloying (MA) methods. The samples were prepared with a ratio of 40 mol% of  $V_2O_5$  and 60 mol% of  $2MnO_2$  and were sintered at different sintering temperatures from 500 to 800°C and characterized. In the meantime, samples of pure oxides, Mn and V were also prepared to compare with the mixed oxides.

X-ray Diffraction confirmed that the samples prepared are multi phases and Rietveld refinement method was employed to estimate the phase composition in each sample. MA method successfully reduced the sintering temperature for the reaction to occur at a much lower temperature compare to SS method. Also, the surfaces of the sample were visualized using Field emission scanning electron microscopy (FESEM) and the average grain size was calculated. From FESEM images, MA method produced very fine particles in nano-scale while SS method in micro-scale.

The DC and AC conductivities of the samples showed the semiconducting behavior because the electrical conductivity increases when temperature increased. The Mn-V oxides have lower electrical conductivity as compare to the starting materials. Since the samples are multi phases, hence the dielectric constant obtained is a contribution from different phases. The polarization mechanism in this frequency region (40 to 1 MHz) can be explained by interfacial and dipolar polarization. On the other hand, the spectra of electric modulus and impedance of the samples successfully revealed the dielectric relaxation process which cannot be observed directly from dielectric loss spectrum. Equivalent circuit modeling was adopted to further describe and predict the electrical

properties of the material. The samples were successfully fitted to single parallel RC circuit or two parallel RC circuits connected in series.

The sample sintered at 500°C prepared using MA method gave the best dielectric properties. This is possibly due to MA method reduces the particle size and increases the grain boundary volume of the sample. Also, the MA series have better thermal stability and gave higher thermal diffusivity compare to SS series where the heat from energy dissipation can be easily transferred for the cooling process.

Lastly, a more comprehensive electrical and thermal study on Mn-V oxide system is done and it can be a reference for future researchers.



Abstrak tesis yang dikemukakan kepada Senat Universiti Putra Malaysia sebagai memenuhi keperluan untuk ijazah Doktor Falsafah

**SIFAT ELEKTRIK BAGI CAMPURAN OKSIDA DARI MANGAN DAN VANADIUM YANG DISEDIAKAN MELALUI KAEDAH PEMROSESAN SERAMIK AND PENGALOIAN MEKANIKAL**

Oleh

**TAN FOO KHOON**

**Jun 2016**

**Pengerusi : Jumiah Hassan, PhD**  
**Fakulti : Institut Teknologi Maju**

Oksida logam mangan (Mn) dan vanadium (V) dikaji secara meluas atas sifat-sifat fizikal asasnya yang menarik. Terdapat beberapa kerja-kerja penyelidikan pada oksida campuran Mn-V dilakukan sebelum ini, tetapi ia masih tidak mempunyai sebuah kajian elektrik yang lengkap mengenai sistem oksida Mn-V yang boleh memberi maklumat lanjut untuk menggambarkan oksida campuran. Dalam projek ini, siasatan terhadap morfologi, kekonduksian elektrik, sifat dielektrik dan kemeresapan terma bagi oksida campuran telah dijalankan. Sampel telah disediakan dengan kaedah pemrosesan seramik (SS) dan pengaloiian mekanik (MA). Sampel telah disediakan dengan nisbah 40 mol% daripada  $V_2O_5$  dan 60 mol% daripada  $2MnO_2$  dan telah disinter pada suhu suhu pensinteran yang berbeza dari 500 hingga 800 °C dan dicirikannya. Pada masa yang sama, sampel-sampel oksida tulen, Mn dan V juga disediakan untuk dibanding dengan oksida campuran.

X-ray Diffraction mengesahkan bahawa sampel yang disediakan adalah dalam pelbagai fasa dan kaedah penyempurnaan Rietveld telah digunakan untuk menganggarkan komposisi fasa dalam setiap sampel. Kaedah MA berjaya mengurangkan suhu pensinteran menyebabkan tindak balas yang berlaku adalah pada suhu yang lebih rendah berbanding dengan kaedah SS. Juga, permukaan sampel itu diperhatikan menggunakan medan imbasan mikroskop elektron (FESEM) dan saiz bijian purata dikira. Daripada imej FESEM, kaedah MA menghasilkan zarah yang sangat halus dalam skala-nano manakala kaedah SS dalam skala-mikro.

Kekonduksian DC dan AC bagi sampel-sampel menunjukkan sifat semikonduktor kerana peningkatan kekonduksian elektrik dengan peningkatan suhu. Oksida Mn-V mempunyai kekonduksian elektrik yang lebih rendah berbanding dengan bahan mentah. Oleh kerana sampel mempunyai pelbagai fasa, maka pemalar dielektrik yang diperolehi adalah dari sumbangan fasa-fasa yang berbeza. Mekanisme polarisasi di julat frekuensi ini (40-1 MHz) dapat dijelaskan oleh polarisasi antaramuka dan dwikutub. Selain itu, modulus elektrik dan impedans sampel berjaya mendedahkan



proses kesantiaan dielektrik yang tidak dapat diperhatikan secara terus daripada spektrum faktor lesapan dielektrik. Pemodelan litar setara telah diggunakan supaya boleh menghurai dan meramalkan sifat-sifat elektrik bagi sesuatu bahan. Sampel-sampel telah berjaya diwakilkan ke satu litar RC selari atau dua litar RC selari disambung secara sesiri.

Sampel disinter pada suhu 500°C disediakan dengan menggunakan kaedah MA mempunyai sifat dielektrik yang terbaik. Ini mungkin disebabkan oleh kaedah MA mengurangkan saiz zarah dan meningkatkan jumlah sempadan bijian dalam sampel. Juga, siri MA yang mempunyai kestabilan terma yang lebih baik dan memberikan kemeresapan terma yang lebih tinggi berbanding dengan siri SS maka haba dibebaskan dari pelepasan tenaga boleh meresap dengan mudah bagi proses penyejukan.

Akhir sekali, kajian elektrik dan haba yang lebih menyeluruh ke atas sistem oksida Mn-V dilakukan dan ia boleh menjadi rujukan kepada penyelidik akan datang.

## ACKNOWLEDGEMENTS

First of all, I would like to express my deepest gratitude and appreciation to my supervisor, Assoc. Prof. Dr. Jumiah Hassan for giving me this opportunity to further my study on materials science by accomplishing this project.

Besides, it is my pleasure to acknowledge my late supervisory committee Assc. Prof. Dr. Mansor Hashim for giving me invaluable advice, guidance, knowledge and help in completing this project. I would also like to extend my sincere appreciation to my third supervisory committee member, Assc. Prof. Dr. Zaidan Wahab for his help and equipment support throughout this project. Also, I would like thank to MyBrain15 - Biasiswa KPM for the 3-year financial support to solve a lot of burden in my daily life.

Special thanks to my lab mates Wong Swee Yin, Alex See, Leow Chun Yan, and Wong Yick Jeng for their advices, help and support during the period of this study. I would like to express my sincere appreciation to the staff and technician of ITMA and also the staff at Faculty of Science for their assistance and guidance.

Finally, I wish to thank my heavenly parents, wife, siblings and my lovely friends for their moral and resources support. Also, thanks to everyone who directly or indirectly bring to the completion of my project.

I certify that a Thesis Examination Committee has met on 8 June 2016 to conduct the final examination of Tan Foo Khoon on his thesis entitled "Electrical Properties of Mixed Oxides of Manganese and Vanadium Prepared by Conventional Solid State and Mechanical Alloying Methods" in accordance with the Universities and University Colleges Act 1971 and the Constitution of the Universiti Putra Malaysia [P.U.(A) 106] 15 March 1998. The Committee recommends that the student be awarded the Doctor of Philosophy.

Members of the Thesis Examination Committee were as follows:

**Suraya binti Abdul Rashid, PhD**

Associate Professor  
Faculty of Engineering  
Universiti Putra Malaysia  
(Chairman)

**Azmi bin Zakaria, PhD**

Professor  
Faculty of Science  
Universiti Putra Malaysia  
(Internal Examiner)

**Halimah binti Mohamed Kamari, PhD**

Associate Professor  
Faculty of Science  
Universiti Putra Malaysia  
(Internal Examiner)

**Raouf Abdle Hamid El-Mallawany, PhD**

Professor  
Menofia University  
Egypt  
(External Examiner)



---

**ZULKARNAIN ZAINAL, PhD**

Professor and Deputy Dean  
School of Graduate Studies  
Universiti Putra Malaysia

Date: 28 September 2016

This thesis was submitted to the Senate of Universiti Putra Malaysia and has been accepted as fulfilment of the requirement for the degree of Doctor of Philosophy. The members of the Supervisory Committee were as follows:

**Jumiah Hassan, PhD**

Associate Professor  
Faculty of Science  
Universiti Putra Malaysia  
(Chairman)

**Zaidan Abdul Wahab, PhD**

Associate Professor  
Faculty of Science  
Universiti Putra Malaysia  
(Member)

---

**BUJANG KIM HUAT, PhD**

Professor and Dean  
School of Graduate Studies  
Universiti Putra Malaysia

Date:

## Declaration by graduate student

I hereby confirm that:

- this thesis is my original work;
- quotations, illustrations and citations have been duly referenced;
- this thesis has not been submitted previously or concurrently for any other degree at any other institutions;
- intellectual property from the thesis and copyright of thesis are fully-owned by Universiti Putra Malaysia, as according to the Universiti Putra Malaysia (Research) Rules 2012;
- written permission must be obtained from supervisor and the office of Deputy Vice-Chancellor (Research and Innovation) before thesis is published (in the form of written, printed or in electronic form) including books, journals, modules, proceedings, popular writings, seminar papers, manuscripts, posters, reports, lecture notes, learning modules or any other materials as stated in theUniversiti Putra Malaysia (Research) Rules 2012;
- there is no plagiarism or data falsification/fabrication in the thesis, and scholarly integrity is upheld as according to the Universiti Putra Malaysia (Graduate Studies) Rules 2003 (Revision 2012-2013) and the Universiti Putra Malaysia (Research) Rules 2012. The thesis has undergone plagiarism detection software.

Signature: \_\_\_\_\_ Date: \_\_\_\_\_

Name and Matric No.: Tan Foo Khoon, GS32277

## Declaration by Members of Supervisory Committee

This is to confirm that:

- the research conducted and the writing of this thesis was under our supervision;
- supervision responsibilities as stated in the Universiti Putra Malaysia (Graduate Studies) Rules 2003 (Revision 2012-2013) are adhered to.

Signature: \_\_\_\_\_  
Name of Chairman of  
Supervisory  
Committee: \_\_\_\_\_

Signature: \_\_\_\_\_  
Name of Member of  
Supervisory  
Committee: \_\_\_\_\_

## TABLE OF CONTENTS

	<b>Page</b>
<b>ABSTRACT</b>	i
<b>ABSTRAK</b>	iii
<b>ACKNOWLEDGEMENTS</b>	v
<b>APPROVAL</b>	vi
<b>DECLARATION</b>	viii
<b>LIST OF TABLES</b>	xiii
<b>LIST OF FIGURES</b>	xv
<b>LIST OF SYMBOLS</b>	xxvii
<b>LIST OF ABBREVIATIONS</b>	xxix
<b>CHAPTER</b>	
<b>1 INTRODUCTION</b>	<b>1</b>
1.1 Background of Project and motivation	1
1.2 Transition Metal	2
1.2.1 Manganese Oxide	2
1.2.2 Vanadium Oxide	3
1.3 Conventional Solid State Method	4
1.4 Mechanical Alloying Method	5
1.5 Objective	5
1.6 Hypothesis	6
1.7 Outline of the Present Study	6
<b>2 LITERATURE REVIEWS</b>	<b>7</b>
2.1 General	7
2.2 Manganese Oxide	7
2.3 Vanadium Oxide	8
2.4 Mn-V Mixed Oxide	10
2.5 Thermal diffusivity	10
2.6 Conventional Solid State Method	11
2.6.1 Mechanisms and Reactions in the Solid State	11
2.6.2 Advantages and Disadvantages of Conventional Solid State Method	12
2.7 Mechanical Alloying Method	13
2.7.1 Mechanisms of Mechanical Alloying	13
2.7.2 Advantages and Disadvantages of Mechanical Alloying Method	15
2.8 Polarization	16
2.8.1 Electronic polarization	16
2.8.2 Ionic polarization	17
2.8.3 Dipolar/Orientation Polarization	17
2.8.4 Interfacial polarization	18
2.8.5 Frequency dependent	19
<b>3 THEORY</b>	<b>21</b>
3.1 General	21
3.2 Mechanism of Sintering	21
3.3 Theory of Dielectric Properties	23

3.3.1	Dielectric	23
3.3.2	Types of Dielectric Materials	24
3.3.3	Electrical Impedance	25
3.3.4	Complex Permittivity	26
3.3.5	Complex Dielectric Modulus	28
3.4	Conductivity	29
3.4.1	DC conductivity	29
3.4.2	AC conductivity	30
3.4.3	Conductivity of Semiconductor	30
3.5	Rietveld Refinement	31
3.6	Thermal Diffusivity	33
<b>4</b>	<b>METHODOLOGY</b>	<b>34</b>
4.1	General	34
4.2	Sample Preparation	35
4.2.1	Flow Chart – Conventional Solid State Method	35
4.2.2	Flow Chart – Mechanical Alloying Method	36
4.2.3	Sample Preparation by Solid State Method	37
4.2.4	Sample Preparation by Mechanical Alloying Method	40
4.3	Metal oxide preparation	42
4.4	Characterization	42
4.4.1	XRD Characterization	42
4.4.2	FESEM Characterization	43
4.4.3	Dielectric Measurement	44
4.4.4	DC Conductivity Measurement	44
4.4.5	Thermal Diffusivity Measurement	45
<b>5</b>	<b>RESULTS AND DISCUSSION</b>	<b>46</b>
5.1	General	46
5.2	XRD	47
5.2.1	Metal Oxide	47
5.2.1.1	Manganese Oxide	47
5.2.1.2	Vanadium Oxide	48
5.2.2	Conventional Solid State Method	49
5.2.3	Mechanical Alloying Method	52
5.3	Microscopic Morphology and Grain Size Analysis	54
5.3.1	Metal Oxide	55
5.3.1.1	Manganese oxide	55
5.3.1.2	Vanadium Oxide	56
5.3.2	Conventional Solid State Method	57
5.3.3	Mechanical Alloying Method	61
5.4	DC Conductivity	65
5.4.1	Metal Oxide	65
5.4.1.1	Manganese oxide	65
5.4.1.2	Vanadium Oxide	66
5.4.2	Conventional Solid State Series	67
5.4.3	Mechanical Alloying Series	69
5.5	AC Conductivity	70
5.5.1	Metal Oxide	70
5.5.1.1	Manganese oxide	70



5.5.1.2	Vanadium Oxide	73
5.5.2	Conventional Solid State Series	75
5.5.3	Mechanical Alloying Series	80
5.6	Activation Energy for DC and AC Conduction	84
5.6.1	Metal Oxide	85
5.6.1.1	Manganese oxide	85
5.6.1.2	Vanadium Oxide	87
5.6.2	Conventional Solid State Series	89
5.6.3	Mechanical Alloying Series	94
5.7	Dielectric Constant, Loss Factor and Loss Tangent	100
5.7.1	Metal Oxide	100
5.7.1.1	Manganese oxide	100
5.7.1.2	Vanadium Oxide	105
5.7.2	Conventional Solid State Series	110
5.7.3	Mechanical Alloying Series	126
5.8	Dielectric Modulus and Activation Energy For Relaxation Process	142
5.8.1	Metal Oxide	142
5.8.1.1	Manganese oxide	142
5.8.1.2	Vanadium Oxide	149
5.8.2	Conventional Solid State Series	154
5.8.3	Mechanical Alloying Series	169
5.9	Impedance Spectroscopy and Equivalent Circuit Modeling	186
5.9.1	Metal Oxide	187
5.9.1.1	Manganese oxide	187
5.9.1.2	Vanadium Oxide	191
5.9.2	Conventional Solid State Series	196
5.9.3	Mechanical Alloying Series	208
5.10	Thermal diffusivity	220
5.10.1	Conventional Solid State Series	220
5.10.2	Mechanical Alloying Series	222
<b>6</b>	<b>CONCLUSION AND SUGGESTIONS</b>	<b>224</b>
6.1	Conclusion	224
6.2	Summary	225
6.3	Suggestions	226
	<b>BIBLIOGRAPHY</b>	<b>227</b>
	<b>APPENDICES</b>	<b>237</b>
	<b>BIODATA OF STUDENT</b>	<b>283</b>
	<b>LIST OF PUBLICATIONS</b>	<b>284</b>

## LIST OF TABLES

<b>Table</b>		<b>Page</b>
2.1	Types of Solid State Heterogeneous Reactions	12
2.2	Milestone in the development of mechanical alloying	13
4.1	List of sample, sintering temperature and pre-sintering temperature of Conventional Solid State Method	40
4.2	List of sample, sintering temperature and pre-sintering temperature of Mechanical alloying method	42
4.3	List of sample, sintering temperature and pre-sintering temperature of Metal oxides	42
4.4	List of constituent compounds in Mn-V oxide	43
5.1	Phase composition of each compound contained in the samples of SS series	51
5.2	Phase composition of each compound contained in the samples of MA series	54
5.3	Average grain size of SS-Mn and MM-Mn	56
5.4	Average grain size of SS-V and MM-V	57
5.5	Aaverage grain size of SS series from 500°C to 800°C	61
5.6	Average grain size of MA series from 500°C to 800°C	64
5.7	Activation energies for DC conduction and pre-exponential factors of SS-Mn and MM-Mn	87
5.8	Activation energies for DC conduction and pre-exponential factors of SS-V and MM-V	89
5.9	Activation energies for DC conduction and pre-exponential factors of SS series	94
5.10	Activation energies for DC conduction and pre-exponential factors of MA series	99
5.11	Relaxation time for SS-Mn and MM-Mn	148
5.12	Activation energy for relaxation time and Debye relaxation time of SS-Mn and MM-Mn	149
5.13	Relaxation time for SS-V and MM-V	153
5.14	Activation energy for relaxation time and Debye relaxation time of SS-V and MM-V	153
5.15	Relaxation time for samples of SS series	168
5.16	Activation energy for relaxation time and Debye relaxation time of samples of SS series	169
5.17	Relaxation time for samples of MA series	185
5.18	Activation energy for Relaxation time and Debye Relaxation time of samples of MA series	185
5.19	Equivalent circuit parameter, relaxation time and $\chi^2$ for SS-Mn	190
5.20	Equivalent circuit parameter, relaxation time and $\chi^2$ for MM-Mn	191

5.21	Equivalent circuit parameter, relaxation time and $\chi^2$ for SS-V	194
5.22	Equivalent circuit parameter, relaxation time and $\chi^2$ for MM-V	195
5.23	Equivalent circuit parameter, relaxation time and $\chi^2$ for SS-500	198
5.24	Equivalent circuit parameter, relaxation time and $\chi^2$ for SS-550	200
5.25	Equivalent circuit parameter, relaxation time and $\chi^2$ for SS-600	201
5.26	Equivalent circuit parameter, relaxation time and $\chi^2$ for SS-650	203
5.27	Equivalent circuit parameter, relaxation time and $\chi^2$ for SS-700	204
5.28	Equivalent circuit parameter, relaxation time and $\chi^2$ for SS-750	206
5.29	Equivalent circuit parameter, relaxation time and $\chi^2$ for SS-800	207
5.30	Equivalent circuit parameter, relaxation time and $\chi^2$ for MA-500	210
5.31	Equivalent circuit parameter, relaxation time and $\chi^2$ for MA - 550	212
5.32	Equivalent circuit parameter, relaxation time and $\chi^2$ for MA - 600	213
5.33	Equivalent circuit parameter, relaxation time and $\chi^2$ for MA - 650	215
5.34	Equivalent circuit parameter, relaxation time and $\chi^2$ for MA - 700	216
5.35	Equivalent circuit parameter, relaxation time and $\chi^2$ for MA - 750	218
5.36	Equivalent circuit parameter, relaxation time and $\chi^2$ for MA - 800	219
A1	Standard Peak List of Manganese (IV) oxide ( $\text{MnO}_2$ )	238
A2	Standard List of Structure of Manganese (IV) oxide ( $\text{MnO}_2$ )	239
A3	Standard Peak List of Vanadium oxide ( $\text{V}_2\text{O}_5$ )	240
A4	Standard List of Structure of Vanadium oxide ( $\text{V}_2\text{O}_5$ )	242
A5	Standard Peak List of Manganese (III) oxide ( $\text{Mn}_2\text{O}_3$ )	243
A6	Standard List of Structure of Manganese (III) oxide ( $\text{Mn}_2\text{O}_3$ )	243
A7	Standard Peak List of Manganese Divanadate ( $\text{MnV}_2\text{O}_6$ )	244
A8	Standard List of Structure of Manganese Divanadate ( $\text{MnV}_2\text{O}_6$ )	246
A9	Standard Peak List of Dimanganese Divanadate-Alpha ( $\alpha\text{-Mn}_2\text{V}_2\text{O}_7$ )	247
A10	Standard List of Structure of Dimanganese Divanadate-Alpha ( $\alpha\text{-Mn}_2\text{V}_2\text{O}_7$ )	252
A11	Standard Peak List of Dimanganese Divanadate-Beta, Ht ( $\beta\text{-Mn}_2\text{V}_2\text{O}_7$ )	253
A12	Standard List of Structure of Dimanganese Divanadate-Beta, Ht ( $\beta\text{-Mn}_2\text{V}_2\text{O}_7$ )	256
A13	List of volume, mass and density of SS-series	263
A14	List of volume, mass and density of MA-series	263

## LIST OF FIGURES

Figure		Page
1.1	Tetragonal crystal system of MnO <sub>2</sub>	3
1.2	Orthorhombic crystal system of V <sub>2</sub> O <sub>5</sub>	4
2.1	Ball-to-ball collision of powder mixture during MA	14
2.2	Electronic Polarization	16
2.3	Ionic Polarization	17
2.4	Dipolar Polarization	18
2.5	Interfacial Polarization	18
2.6	Variation of the dielectric constant, loss factor and types of polarization with frequency	20
3.1	Schematic diagram of three-particle model after sintering process	22
3.2	Schematic diagram of two particles undergo sintering process	22
3.3	Examples of microstructure image for (a) initial stage, (b) intermediate stage, and (c) final stage of sintering	22
3.4	Room temperature conductivity of various materials	23
3.5	Band theory for conduction in metals, semiconductors and insulators	24
3.6	Model of (a) non-polar molecule, (b) the molecule in an external electric field	24
3.7	Model of unpolarized polar molecules and polarized polar molecules	25
3.8	Relationships between resistive current and applied voltage	28
3.9	Equivalent circuit for ideal spectra of dielectric modulus vs frequency	29
3.10	Typical log conductivity varies with reciprocal temperature curve for an extrinsic semiconductor	31
4.1	Research flow chart	34
4.2	Flow chart of sample preparation by using conventional solid state method	36
4.3	Flow chart of sample preparation by using mechanical alloying method	37
4.4	Electrical circuit set up for conductivity measurement	44
5.1	XRD Patterns of Manganese(III) Oxide-beta, Manganese(IV) Oxide-beta, SS-Mn and MM-Mn	48
5.2	XRD Patterns of V <sub>2</sub> O <sub>5</sub> , SS-V and MM-V	49
5.3	XRD patterns of SS series	51
5.4	Variation of phase composition of each compound in SS series with respect to sintering temperature	52
5.5	XRD patterns of MA series	53

5.6	Variation of phase composition of each compound in MA series with respect to sintering temperature	54
5.7	FESEM images and grains size distribution for a) SS-Mn, b) MM-Mn	55
5.8	FESEM images and grains size distribution for a) SS-V, FESEM image and V <sub>2</sub> O <sub>5</sub> belt length distribution for b) MM-V	57
5.9	FESEM images and grains size distribution for (a) SS-500, (b) SS-550, (c) SS-600, (d) SS-650, (e) SS-700, (f) SS-750 and (g) SS-800	60
5.10	FESEM images and grains size distribution for (a) MA-500, (b) MA -550, (c) MA -600, (d) MA -650, (e) MA -700, (f) MA -750 and (g) MA -800	64
5.11	Variation of DC conductivity with respect to measuring temperatures from 30°C to 250°C for SS-Mn and MM-Mn	66
5.12	Variation of DC conductivity with respect to measuring temperatures from 30°C to 250°C for SS-V and MM-V	67
5.13	Variation of DC conductivity with respect to measuring temperatures from 30°C to 250°C for SS series	69
5.14	Variation of DC conductivity with respect to measuring temperatures from 30°C to 250°C for MA series	70
5.15	Variation of AC conductivity with respect to frequency at different measuring temperatures from 30°C to 250°C for SS-Mn	72
5.16	Variation of AC conductivity with respect to frequency at different measuring temperatures from 30°C to 250°C for MM-Mn	72
5.17	Variation of AC conductivity with respect to frequency at different measuring temperatures from 30°C to 250°C for SS-V	74
5.18	Variation of AC conductivity with respect to frequency at different measuring temperatures from 30°C to 250°C for MM-V	74
5.19	Variation of AC conductivity with respect to frequency at different measuring temperatures from 30°C to 250°C for SS-500	76
5.20	Variation of AC conductivity with respect to frequency at different measuring temperatures from 30°C to 250°C for SS-550	77
5.21	Variation of AC conductivity with respect to frequency at different measuring temperatures from 30°C to 250°C for SS-600	77

5.22	Variation of AC conductivity with respect to frequency at different measuring temperatures from 30°C to 250°C for SS-650	78
5.23	Variation of AC conductivity with respect to frequency at different measuring temperatures from 30°C to 250°C for SS-700	78
5.24	Variation of AC conductivity with respect to frequency at different measuring temperatures from 30°C to 250°C for SS-750	79
5.25	Variation of AC conductivity with respect to frequency at different measuring temperatures from 30°C to 250°C for SS-800	79
5.26	Variation of AC conductivity with respect to frequency at different measuring temperatures from 30°C to 250°C for MA-500	81
5.27	Variation of AC conductivity with respect to frequency at different measuring temperatures from 30°C to 250°C for MA-550	81
5.28	Variation of AC conductivity with respect to frequency at different measuring temperatures from 30°C to 250°C for MA-600	82
5.29	Variation of AC conductivity with respect to frequency at different measuring temperatures from 30°C to 250°C for MA-650	82
5.30	Variation of AC conductivity with respect to frequency at different measuring temperatures from 30°C to 250°C for MA-700	83
5.31	Variation of AC conductivity with respect to frequency at different measuring temperatures from 30°C to 250°C for MA-750	83
5.32	Variation of AC conductivity with respect to frequency at different measuring temperatures from 30°C to 250°C for MA-800	84
5.33	Temperature dependence of $\ln \sigma_{ac}$ of SS-Mn at different frequencies; the inset figure represents the plot of $\Delta E_{ac}$ versus frequency	86
5.34	Temperature dependence of $\ln \sigma_{ac}$ of MM-Mn at different frequencies; the inset figure represents the plot of $\Delta E_{ac}$ versus frequency	86
5.35	Temperature dependence of $\ln \sigma_{ac}$ of SS-V at different frequencies; the inset figure represents the plot of $\Delta E_{ac}$ versus frequency	88

5.36	Temperature dependence of $\ln \sigma_{ac}$ of MM-V at different frequencies; the inset figure represents the plot of $\Delta E_{ac}$ versus frequency	88
5.37	Temperature dependence of $\ln \sigma_{ac}$ of SS-500 at different frequencies; the inset figure represents the plot of $\Delta E_{ac}$ versus frequency	90
5.38	Temperature dependence of $\ln \sigma_{ac}$ of SS-550 at different frequencies; the inset figure represents the plot of $\Delta E_{ac}$ versus frequency	91
5.39	Temperature dependence of $\ln \sigma_{ac}$ of SS-600 at different frequencies; the inset figure represents the plot of $\Delta E_{ac}$ versus frequency	92
5.40	Temperature dependence of $\ln \sigma_{ac}$ of SS-650 at different frequencies; the inset figure represents the plot of $\Delta E_{ac}$ versus frequency	92
5.41	Temperature dependence of $\ln \sigma_{ac}$ of SS-700 at different frequencies; the inset figure represents the plot of $\Delta E_{ac}$ versus frequency	93
5.42	Temperature dependence of $\ln \sigma_{ac}$ of SS-750 at different frequencies; the inset figure represents the plot of $\Delta E_{ac}$ versus frequency	93
5.43	Temperature dependence of $\ln \sigma_{ac}$ of SS-800 at different frequencies; the inset figure represents the plot of $\Delta E_{ac}$ versus frequency	94
5.44	(a) Arrhenius plots of $\ln \sigma_{ac}$ of MA-500 at different frequencies; the inset figure represents the plot of $\Delta E_{ac}$ versus frequency, (b) Plot of $\Delta E_{ac}$ versus frequency due to extrinsic properties.	96
5.45	Temperature dependence of $\ln \sigma_{ac}$ of MA-550 at different frequencies; the inset figure represents the plot of $\Delta E_{ac}$ versus frequency	96
5.46	Temperature dependence of $\ln \sigma_{ac}$ of MA-600 at different frequencies; the inset figure represents the plot of $\Delta E_{ac}$ versus frequency	97
5.47	Temperature dependence of $\ln \sigma_{ac}$ of MA-650 at different frequencies; the inset figure represents the plot of $\Delta E_{ac}$ versus frequency	97
5.48	Temperature dependence of $\ln \sigma_{ac}$ of MA-700 at different frequencies; the inset figure represents the plot of $\Delta E_{ac}$ versus frequency	98
5.49	Temperature dependence of $\ln \sigma_{ac}$ of MA-750 at different frequencies; the inset figure represents the plot of $\Delta E_{ac}$ versus frequency	98

5.50	Temperature dependence of $\ln \sigma_{ac}$ of MA-800 at different frequencies; the inset figure represents the plot of $\Delta E_{ac}$ versus frequency	99
5.51	Frequency dependence of (a) dielectric constant, (b) dielectric loss factor and (c) loss tangent for SS-Mn at different measuring temperatures; and (d) Temperature dependence of dielectric constant at different frequencies	102
5.52	Frequency dependence of (a) dielectric constant, (b) dielectric loss factor and (c) loss tangent for MM-Mn at different measuring temperatures; and (d) Temperature dependence of dielectric constant at different frequencies	104
5.53	Frequency dependence of (a) dielectric constant, (b) dielectric loss factor and (c) loss tangent for SS-V at different measuring temperatures and (d) Temperature dependence of dielectric constant at different frequencies	107
5.54	Frequency dependence of (a) dielectric constant, (b) dielectric loss factor and (c) loss tangent for MM-V at different measuring temperatures and (d) Temperature dependence of dielectric constant at different frequencies	109
5.55	Frequency dependence of (a) dielectric constant, (b) dielectric loss factor and (c) loss tangent for SS-500 at different measuring temperatures; and (d) Temperature dependence of dielectric constant at different frequencies	113
5.56	Frequency dependence of (a) dielectric constant, (b) dielectric loss factor and (c) loss tangent for SS-550 at different measuring temperatures; and (d) Temperature dependence of dielectric constant at different frequencies	115
5.57	Frequency dependence of (a) dielectric constant, (b) dielectric loss factor and (c) loss tangent for SS-600 at different measuring temperatures; and (d) Temperature dependence of dielectric constant at different frequencies	117
5.58	Frequency dependence of (a) dielectric constant, (b) dielectric loss factor and (c) loss tangent for SS-650 at different measuring temperatures; and (d) Temperature dependence of dielectric constant at different frequencies	119
5.59	Frequency dependence of (a) dielectric constant, (b) dielectric loss factor and (c) loss tangent for SS-700 at different measuring temperatures; and (d) Temperature dependence of dielectric constant at different frequencies	121
5.60	Frequency dependence of (a) dielectric constant, (b) dielectric loss factor and (c) loss tangent for SS-750 at different measuring temperatures; and (d) Temperature dependence of dielectric constant at different frequencies	123



5.61	Frequency dependence of (a) dielectric constant, (b) dielectric loss factor and (c) loss tangent for SS-800 at different measuring temperatures; and (d) Temperature dependence of dielectric constant at different frequencies	125
5.62	Frequency dependence of (a) dielectric constant, (b) dielectric loss factor and (c) loss tangent for MA-500 at different measuring temperatures; and (d) Temperature dependence of dielectric constant at different frequencies	129
5.63	Frequency dependence of (a) dielectric constant, (b) dielectric loss factor and (c) loss tangent for MA -550 at different measuring temperatures; and (d) Temperature dependence of dielectric constant at different frequencies	131
5.64	Frequency dependence of (a) dielectric constant, (b) dielectric loss factor and (c) loss tangent for MA -600 at different measuring temperatures; and (d) Temperature dependence of dielectric constant at different frequencies	133
5.65	Frequency dependence of (a) dielectric constant, (b) dielectric loss factor and (c) loss tangent for MA -650 at different measuring temperatures; and (d) Temperature dependence of dielectric constant at different frequencies	135
5.66	Frequency dependence of (a) dielectric constant, (b) dielectric loss factor and (c) loss tangent for MA -700 at different measuring temperatures; and (d) Temperature dependence of dielectric constant at different frequencies	137
5.67	Frequency dependence of (a) dielectric constant, (b) dielectric loss factor and (c) loss tangent for MA -750 at different measuring temperatures; and (d) Temperature dependence of dielectric constant at different frequencies	139
5.68	Frequency dependence of (a) dielectric constant, (b) dielectric loss factor and (c) loss tangent for MA -800 at different measuring temperatures; and (d) Temperature dependence of dielectric constant at different frequencies	141
5.69	Frequency dependence of (a) imaginary part of modulus, (b) Complex plane of complex electric modulus, (c) plot of $Im\tau$ versus $1000/T$ for SS-Mn at different measuring temperature	145
5.70	Frequency dependence of (a) imaginary part of modulus, (b) Complex plane of complex electric modulus, (c) plot of $Im\tau$ versus $1000/T$ for MM-Mn at different measuring temperature	148
5.71	Frequency dependence of (a) imaginary part of modulus, (b) Complex plane of complex electric modulus, (c) plot of $Im\tau$ versus $1000/T$ for SS-V at different measuring temperature	151

5.72	Frequency dependence of (a) imaginary part of modulus, (b) Complex plane of complex electric modulus for MM-V at different measuring temperature	153
5.73	Frequency dependence of (a) imaginary part of modulus, (b) Complex plane of complex electric modulus for SS-500 at different measuring temperature	156
5.74	Frequency dependence of (a) imaginary part of modulus, (b) Complex plane of complex electric modulus for SS-550 at different measuring temperature	158
5.75	Frequency dependence of (a) imaginary part of modulus, (b) Complex plane of complex electric modulus, (c) plot of $Int$ versus $1000/T$ for SS-600 at different measuring temperature	160
5.76	Frequency dependence of (a) imaginary part of modulus, (b) Complex plane of complex electric modulus, (c) plot of $Int$ versus $1000/T$ for SS-650 at different measuring temperature	162
5.77	Frequency dependence of (a) imaginary part of modulus, (b) Complex plane of complex electric modulus, (c) plot of $Int$ versus $1000/T$ for SS-700 at different measuring temperature	164
5.78	Frequency dependence of (a) imaginary part of modulus, (b) Complex plane of complex electric modulus, (c) plot of $Int$ versus $1000/T$ for SS-750 at different measuring temperature	166
5.79	Frequency dependence of (a) imaginary part of modulus, (b) Complex plane of complex electric modulus, (c) plot of $Int$ versus $1000/T$ for SS-800 at different measuring temperature	168
5.80	Frequency dependence of (a) imaginary part of modulus, (b) Complex plane of complex electric modulus, (c) plot of $Int$ versus $1000/T$ for MA-500 at different measuring temperature	172
5.81	Frequency dependence of (a) imaginary part of modulus, (b) Complex plane of complex electric modulus, (c) plot of $Int$ versus $1000/T$ for MA-550 at different measuring temperature	174
5.82	Frequency dependence of (a) imaginary part of modulus, (b) Complex plane of complex electric modulus, (c) plot of $Int$ versus $1000/T$ for MA-600 at different measuring temperature	176
5.83	Frequency dependence of (a) imaginary part of modulus, (b) Complex plane of complex electric modulus, (c) plot of $Int$ versus $1000/T$ for MA-650 at different measuring temperature	178
5.84	Frequency dependence of (a) imaginary part of modulus, (b) Complex plane of complex electric modulus, (c) plot of $Int$ versus $1000/T$ for MA-700 at different measuring temperature	180

5.85	Frequency dependence of (a) imaginary part of modulus, (b) Complex plane of complex electric modulus, (c) plot of $Im\tau$ versus $1000/T$ for MA-750 at different measuring temperature	182
5.86	Frequency dependence of (a) imaginary part of modulus, (b) Complex plane of complex electric modulus, (c) plot of $Im\tau$ versus $1000/T$ for MA-800 at different measuring temperature	184
5.87	Two parallel R and CPE circuits connected in series where $g$ and $g_b$ represent grain and grain boundary respectively	187
5.88	Frequency dependence of (a) imaginary part of impedance, (b) Nyquist plot of complex impedance for SS-Mn at different measuring temperatures.	189
5.89	Frequency dependence of (a) imaginary part of impedance, (b) Nyquist plot of complex impedance for MM-Mn at different measuring temperatures.	191
5.90	Frequency dependence of (a) imaginary part of impedance, (b) Nyquist plot of complex impedance for SS-V at different measuring temperatures.	193
5.91	Frequency dependence of (a) imaginary part of impedance, (b) Nyquist plot of complex impedance for MM-V at different measuring temperatures.	195
5.92	Frequency dependence of (a) imaginary part of impedance, (b) Nyquist plot of complex impedance for SS-500 at different measuring temperatures.	198
5.93	Frequency dependence of (a) imaginary part of impedance, (b) Nyquist plot of complex impedance for SS-550 at different measuring temperatures.	199
5.94	Frequency dependence of (a) imaginary part of impedance, (b) Nyquist plot of complex impedance for SS-600 at different measuring temperatures.	201
5.95	Frequency dependence of (a) imaginary part of impedance, (b) Nyquist plot of complex impedance for SS-650 at different measuring temperatures.	202
5.96	Frequency dependence of (a) imaginary part of impedance, (b) Nyquist plot of complex impedance for SS-700 at different measuring temperatures.	204
5.97	Frequency dependence of (a) imaginary part of impedance, (b) Nyquist plot of complex impedance for SS-750 at different measuring temperatures.	205
5.98	Frequency dependence of (a) imaginary part of impedance, (b) Nyquist plot of complex impedance for SS-800 at different measuring temperatures.	207

5.99	Frequency dependence of (a) imaginary part of impedance, (b) Nyquist plot of complex impedance for MA-500 at different measuring temperatures.	210
5.100	Frequency dependence of (a) imaginary part of impedance, (b) Nyquist plot of complex impedance for MA-550 at different measuring temperatures.	211
5.101	Frequency dependence of (a) imaginary part of impedance, (b) Nyquist plot of complex impedance for MA-600 at different measuring temperatures.	213
5.102	Frequency dependence of (a) imaginary part of impedance, (b) Nyquist plot of complex impedance for MA-650 at different measuring temperatures.	214
5.103	Frequency dependence of (a) imaginary part of impedance, (b) Nyquist plot of complex impedance for MA-700 at different measuring temperatures.	216
5.104	Frequency dependence of (a) imaginary part of impedance, (b) Nyquist plot of complex impedance for MA-750 at different measuring temperatures.	217
5.105	Frequency dependence of (a) imaginary part of impedance, (b) Nyquist plot of complex impedance for MA-800 at different measuring temperatures.	219
5.106	Temperature dependence of thermal diffusivity for SS-500, SS-550 and SS-600	221
5.107	Temperature dependence of thermal diffusivity for SS-650, SS-700, SS-750 and SS-800	221
5.108	Temperature dependence of thermal diffusivity for MA-500, MA-550 and MA-600	223
5.109	Temperature dependence of thermal diffusivity for MA-650, MA-700, MA-750 and MA-800	223
A1	Standard Stick Pattern of Manganese (IV) oxide (MnO <sub>2</sub> )	239
A2	Standard Stick Pattern of Vanadium oxide (V <sub>2</sub> O <sub>5</sub> )	242
A3	Standard Stick Pattern of Manganese (III) oxide (Mn <sub>2</sub> O <sub>3</sub> )	244
A4	Standard Stick Pattern of Manganese Divanadate (MnV <sub>2</sub> O <sub>6</sub> )	247
A5	Standard Stick Pattern of Dimanganese Divanadate-Alpha ( $\alpha$ -Mn <sub>2</sub> V <sub>2</sub> O <sub>7</sub> )	252
A6	Standard Stick Pattern of Dimanganese Divanadate-Beta, Ht ( $\beta$ -Mn <sub>2</sub> V <sub>2</sub> O <sub>7</sub> )	256
A7	XRD pattern for SS-700	257
A8	XRD pattern for SS-750	257
A9	XRD pattern for SS-800	258
A10	FESEM images of SS-500 (a) 10 kx (b) 25 kx (c) 50 kx magnification	259
A11	FESEM images of SS-550 (a) 10 kx (b) 25 kx (c) 50 kx magnification	259

A12	FESEM images of SS-600 (a) 10 kx (b) 25 kx (c) 50 kx magnification	259
A13	FESEM images of SS-650 (a) 10 kx (b) 25 kx magnification	260
A14	FESEM images of SS-700 (a) 5 kx (b) 10 kx (c) 25 kx magnification	260
A15	FESEM images of SS-750 (a) 5 kx (b) 10 kx magnification	260
A16	FESEM images of SS-800 (a) 5 kx (b) 10 kx magnification	260
A17	FESEM images of MA-500 (a) 10 kx (b) 50 kx (c) 100 kx magnification	261
A18	FESEM images of MA-550 (a) 10 kx (b) 50 kx (c) 100 kx magnification	261
A19	FESEM images of MA-600 (a) 10 kx (b) 25 kx (c) 50 kx magnification	261
A20	FESEM images of MA-650 (a) 10 kx (b) 25 kx (c) 50 kx magnification	262
A21	FESEM images of MA-700 (a) 10 kx (b) 25 kx (c) 50 kx magnification	262
A22	FESEM images of MA-750 (a) 10 kx (b) 20 kx (c) 50 kx magnification	262
A23	FESEM images of MA-800 (a) 10 kx (b) 20 kx (c) 50 kx magnification	262
A24	SPEX SamplePrep 8000D Mixer/Mill	264
A25	Vial and grinding balls	264
A26	Frequency dependence of real part of electric modulus for SS-Mn at different measuring frequencies.	265
A27	Frequency dependence of real part of electric modulus for MM-Mn at different measuring frequencies.	265
A28	Frequency dependence of real part of electric modulus for SS-V at different measuring frequencies.	266
A29	Frequency dependence of real part of electric modulus for MM-V at different measuring frequencies.	266
A30	Frequency dependence of real part of electric modulus for SS-500 at different measuring frequencies.	267
A31	Frequency dependence of real part of electric modulus for SS-550 at different measuring frequencies.	267
A32	Frequency dependence of real part of electric modulus for SS-600 at different measuring frequencies.	268
A33	Frequency dependence of real part of electric modulus for SS-650 at different measuring frequencies.	268
A34	Frequency dependence of real part of electric modulus for SS-700 at different measuring frequencies.	269
A35	Frequency dependence of real part of electric modulus for SS-750 at different measuring frequencies.	269

A36	Frequency dependence of real part of electric modulus for SS-800 at different measuring frequencies.	270
A37	Frequency dependence of real part of electric modulus for MA-500 at different measuring frequencies.	270
A38	Frequency dependence of real part of electric modulus for MA-550 at different measuring frequencies.	271
A39	Frequency dependence of real part of electric modulus for MA-600 at different measuring frequencies.	271
A40	Frequency dependence of real part of electric modulus for MA-650 at different measuring frequencies.	272
A41	Frequency dependence of real part of electric modulus for MA-700 at different measuring frequencies.	272
A42	Frequency dependence of real part of electric modulus for MA-750 at different measuring frequencies.	273
A43	Frequency dependence of real part of electric modulus for MA-800 at different measuring frequencies.	273
A44	Frequency dependence of real part of complex impedance for SS-Mn at different measuring frequencies.	274
A45	Frequency dependence of real part of complex impedance for MM-Mn at different measuring frequencies.	274
A46	Frequency dependence of real part of complex impedance for SS-V at different measuring frequencies.	275
A47	Frequency dependence of real part of complex impedance for MM-V at different measuring frequencies.	275
A48	Frequency dependence of real part of complex impedance for SS-500 at different measuring frequencies.	276
A49	Frequency dependence of real part of complex impedance for SS-550 at different measuring frequencies.	276
A50	Frequency dependence of real part of complex impedance for SS-600 at different measuring frequencies.	277
A51	Frequency dependence of real part of complex impedance for SS-650 at different measuring frequencies.	277
A52	Frequency dependence of real part of complex impedance for SS-700 at different measuring frequencies.	278
A53	Frequency dependence of real part of complex impedance for SS-750 at different measuring frequencies.	278
A54	Frequency dependence of real part of complex impedance for SS-800 at different measuring frequencies.	279
A55	Frequency dependence of real part of complex impedance for MA-500 at different measuring frequencies.	279
A56	Frequency dependence of real part of complex impedance for MA-550 at different measuring frequencies.	280
A57	Frequency dependence of real part of complex impedance for MA-600 at different measuring frequencies.	280

A58	Frequency dependence of real part of complex impedance for MA-650 at different measuring frequencies.	281
A59	Frequency dependence of real part of complex impedance for MA-700 at different measuring frequencies.	281
A60	Frequency dependence of real part of complex impedance for MA-750 at different measuring frequencies.	282
A61	Frequency dependence of real part of complex impedance for MA-800 at different measuring frequencies.	282



## LIST OF SYMBOLS

$C$	Capacitance
$C_{gb}$	Grain boundary capacitance
$C_g$	Grain capacitance
$F$	Farad
$R$	Resistance
$R_{gb}$	Grain boundary resistance
$R_g$	Grain resistance
$\Omega$	Ohm
$G$	Conductance
$f$	Frequency
$I$	Current
$E$	Electric field
$\sigma$	Magnitude of surface charge density
$Q$	Magnitude of total charge
$V$	Potential difference
$A$	Area of each plate or cross-sectional area
$d$	Separation between the plates
$C_o$	Capacitance of parallel plates in vacuum
$\epsilon_0$	Permittivity of free space
$\epsilon^*$	Complex permittivity
$\epsilon_r^*$	Relative complex permittivity
$\epsilon_r'$	Relative dielectric constant
$\epsilon_r''$	Relative dielectric loss factor
$\tan \delta$	Dielectric loss tangent
$I_{cal}$	Calculated intensity
$hkl$	Miller Indexes
$C_{hkl}$	Correction due to experimental geometry set-up
$F_{hkl}^2$	Structure factor
$I_{bck}$	Refinement Parameter: Background
$P_{hkl}$	Refinement Parameter: Peak Profile
$\omega$	Angular frequency
$\omega$	Angular frequency
$\omega_{max}$	Angular frequency at corresponding peak
$X$	Reactance
$j$	Imaginary part, $\sqrt{-1}$
$Z^*$	Complex Impedance
$Z'$	Real part of impedance
$Z''$	Imaginary part of impedance
$M^*$	Complex electric modulus
$M'$	Real part of electric modulus
$M''$	Imaginary part of electric modulus



$M_{max}$	the value of $M''$ peak
$f_M$	Peak frequency
$Y^*$	Complex admittance
$Y'$	Real part of admittance
$Y''$	Imaginary part of admittance
$\chi_e$	Dielectric susceptibility of the medium
$\chi_e$	Dielectric susceptibility of the medium
$l$	Length
$\rho$	Resistivity
$\sigma$	Conductivity
$\sigma_{dc}$	DC conductivity
$\sigma_{ac}$	AC conductivity
$s$	Frequency exponent
$E_g$	Energy gap
$K$	Thermal conductivity
$\alpha$	Thermal diffusivity
$\rho$	Density
$c$	Specific heat capacity
$\dot{Q}$	Heat transfer
$T$	Temperature, K
wt%	Weight percentage
mol%	Mol percentage
$W_i$	Weight fraction
$S_i$	Scale factor of phase $i$
$Z$	Number of formula units per unit cell
$M$	Mass of the formula unit
$V$	Volume of the unit cell
$\Delta E$	Activation Energy
$\Delta E_{dc}$	Activation Energy for DC conduction
$\Delta E_{ac}$	Activation Energy for AC conduction
$K_B$	Boltzmann constant
$\sigma_o$	Pre-exponential factor
$\tau$	Relaxation time
$\tau_o$	Pre-exponential factor or the relaxation time at infinite temperature
$\tau_{gb}$	Grain boundary relaxation time
$\tau_g$	Grain relaxation time
$\Delta E_R$	Activation energy of relaxation process
$Y_o, n$	Parameter of CPE
$\chi^2$	Chi square

## LIST OF ABBREVIATIONS

SS	Conventional solid state
MA	Mechanical alloying
MM	Mechanical milling
MnO <sub>2</sub>	Manganese (IV) oxide
Mn <sub>2</sub> O <sub>3</sub>	Manganese (III) oxide
V <sub>2</sub> O <sub>5</sub>	Vanadium pentoxide
XRD	X-ray diffraction
FESEM	Field emission scanning electron microscopy
PVA	Polyvinyl alcohol
ICSD	Inorganic Crystal Structure Database
AC	Alternating current
DC	Direct current
g	Grain
gb	Grain boundary
CPE	Constant phase element

# CHAPTER 1

## INTRODUCTION

### 1.1 Background of project and motivation

Currently, composite materials have wide variety of applications in our daily life such as electrical devices, mobile communication systems, etc. Therefore, composite tailoring was set off to suit the particular needs for different usages.

In the past decade, there have been several research carried out with different metal oxides due to their applications in various electronic devices such as smart window (Zhangli et al., 2013), optical detector (Bin et al., 2013), cathode coating in high-capacity lithium batteries (Di Blasi et al., 2015), high performance capacitor (Vilar et al., 2005), thermistor (Gouda et al., 2013) and others.

Transition element has mixed valence ions, hence those compounds have unique properties and very useful in various fields. Manganese is one of the transition element which has a formal oxidation state from -3 to +7. Meanwhile, manganese oxides include MnO, Mn<sub>2</sub>O<sub>3</sub>, Mn<sub>2</sub>O<sub>7</sub>, etc (Kemmitt et al., 1975). According to pervious researches, composites containing MnO<sub>2</sub> such as V<sub>2</sub>O<sub>5</sub> (Gouda et al., 2009), SnO, As<sub>2</sub>O<sub>3</sub> (Kayan et al., 2004), CaO (Vilar et al., 2005), Fe<sub>2</sub>O<sub>3</sub> (Molenda et al., 1987) etc were investigated.

Besides, vanadium oxides which include V<sub>2</sub>O<sub>3</sub>, V<sub>2</sub>O<sub>5</sub>, V<sub>6</sub>O<sub>13</sub>, VO<sub>2</sub>, etc., show a phase transition from the semiconductor phase to the metal phase when measuring temperature increases (Xiaochun et al., 2008). Therefore, the phase change gives more variations of electrical and dielectric properties.

From previous study, Gouda et al. (Gouda et al., 2009) prepared mixed oxides of Mn and V under different mass ratio of Mn<sub>2</sub>O<sub>3</sub> and VO<sub>2</sub> from 90:10 to 5:95. They found that resistivity and thermistor constant of beta or gamma form of Mn<sub>2</sub>V<sub>2</sub>O<sub>7</sub> are higher compared to the well known oxides of vanadium and binary/ternary oxides of manganese, nickel and cobalt. It meant that d-block electronic configuration of V<sup>5+</sup> in Mn<sub>2</sub>V<sub>2</sub>O<sub>7</sub> contributed to higher resistivity (Bordeneuve et al., 2009).

There were some works related with V<sub>2</sub>O<sub>5</sub> done previously, but the reports were focused on structural investigation and some electrical properties of MnV<sub>2</sub>O<sub>6</sub> and Mn<sub>2</sub>V<sub>2</sub>O<sub>7</sub> (Gouda et al., 2013; Gouda et al., 2009; Dongfang, 2013; Mocala et al., 1987). However, it still lacks a comprehensive electrical studies on Mn-V oxide system which can gives insight into the response of grain and grain boundary to the electric field. Also, there were several investigations related to Mn and V oxides reported prepared by different methods which were pulsed laser deposition (Dongfang, 2013), solid state reaction (Gouda et al., 2009, Mocala et al., 1987) and high pressure synthesis (Subramanian,

1992). However, there are no studies on Mn-V oxide prepared by mechanical alloying method. Therefore, it is a pioneer work in this project. According to previous studies, the Mn-V mixed oxides prepared in this project may have high dielectric loss factor and the energy loss may convert into heat. Hence, thermal diffusivity measurement was carried out to further understand the thermal properties of the mixed oxides.

In this project, the conventional solid state and mechanical alloying method were employed to prepare the samples. The aim is confined to study the morphology and the phase composition of Mn-V oxides produced at different sintering temperatures. Also, the electrical and dielectric properties of the mixed oxides at different measuring temperature were also investigated. Lastly, the thermal diffusivity of the mixed oxides was measured at different temperatures as subordinate studies in this project.

## **1.2 Transition Metal**

In the periodic table, the transition metals are any element in d-block of the periodic table. These elements have partially filled d sub-shell which can give up their valence electrons to become cation. Therefore, the d-orbitals have variety of oxidation states.

The general properties of the transition metals are usually high melting point, have several oxidation states, form coloured compounds and paramagnetic (HyperPhysics, n.d.). Transition metal oxides are starting to draw attention from many researchers, because they have wide range of electronic properties ranging from insulating, semiconductor and conducting properties. Their electronic properties can be modified by changing its morphology structure, doping or changing their stoichiometry. The plentiful of transition metal oxides in nature is another advantage for technologies to be widely utilized (Walia et al., 2013).

### **1.2.1 Manganese Oxide**

Manganese element is one of a transition metal which is hard and bronze in color. It is one of the transition elements which have a wide range of oxidation states such as +2, +3, +4, +6, and +7. The electron configuration of manganese element is  $1s^2 2s^2 2p^6 3s^2 3p^6 4s^2 3d^5$ . The melting point of manganese metal is relatively high which is 1244 °C (Kemmitt et al., 1975). It occurs naturally as the mineral pyrolusite, which is an essential ore of manganese (Anthony et al., 1990). On the other hand, manganese oxides basically include MnO, Mn<sub>3</sub>O<sub>4</sub>, Mn<sub>2</sub>O<sub>3</sub>, MnO<sub>2</sub> with different allotropes which show some advantages of non-toxicity, easy to obtain and therefore low cost. Moreover, they exhibit high specific capacitances and have become the most promising materials in application of supercapacitors (Junhua et al., 2002).

Manganese (IV) oxide is the one of the starting materials in this project. It is also known as manganese dioxide, MnO<sub>2</sub> with +4 oxidation state. MnO<sub>2</sub> has blackish or brown solid physical appearance. MnO<sub>2</sub> melts at 535°C (MSDS, n.d.) and insoluble in water. The

basic unit of  $\text{MnO}_2$  is octahedral closed packet structure, which is built up by one manganese atom coordinated with six oxygen atoms (Figure 1.1). The atoms are linked together in different ways so as to form various crystallographic and derivative structures (Inorganic Crystal Structure Database, 2014).

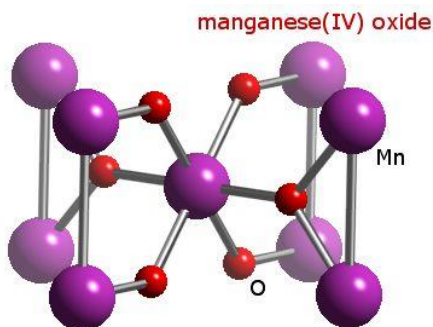


**Figure 1.1: Tetragonal crystal system of  $\text{MnO}_2$ .**

([http://www.webelements.com/compounds/manganese/manganese\\_dioxide.html](http://www.webelements.com/compounds/manganese/manganese_dioxide.html))

Naturally,  $\text{MnO}_2$  with different structural forms has been found, which are  $\alpha$ -,  $\beta$ -,  $\delta$ -,  $\gamma$ - and  $\epsilon$ - $\text{MnO}_2$  which have various properties (Zhong Jie et al., 2015; Hongtao et al., 2012). The  $\alpha$ - $\text{MnO}_2$  phase has nanowire structure where  $\beta$ - $\text{MnO}_2$  phase has microrods structure (Bang et al., 2014). The different morphologies structures of manganese oxide can result in the change of crystal lattice, the differences of crystal defects and holes, which affect the polarization and consequently alter the dielectric properties of materials. According to the morphological structure, microrods have less polarization ability than nanowires, hence  $\alpha$ - $\text{MnO}_2$  has higher dielectric permittivity compared  $\beta$ - $\text{MnO}_2$ . Also, the temperature will affect the movement of charge carriers in the interior tunnels and cavities which leads to the fact that  $\text{MnO}_2$  materials will have various dielectric relaxation phenomena and electromagnetic characteristics (Yude et al., 2010; Hongtao et al., 2010).

Nowadays,  $\text{MnO}_2$  is widely studied because of its interesting fundamental physical properties. They have lots of applications such as, catalyst, molecular-sieves, ion-sieves due to its ion exchange, molecular adsorption, electrochemical and magnetic properties (Yude et al., 2010). It is also used in preparing soft magnetic materials, electrodes and electrochemical capacitors (Dakhel, 2006).

### 1.2.2 Vanadium Oxide

Vanadium element has an atomic number of 23 and the electronic configuration is  $1s^2 2s^2 2p^6 3s^2 3p^6 4s^2 3d^3$ . Vanadium element is a transition metal element which has variation of oxidation states ranging from +5, +4, +3 to +2. Therefore, it exists in many phases such as VO,  $\text{VO}_2$ ,  $\text{V}_2\text{O}_3$  or  $\text{V}_2\text{O}_5$  (Walia, et al. 2013).  $\text{V}_2\text{O}_5$  is a brown or yellow solid. It is an amphoteric oxide and oxidizing agent (Zabriky, 2009).

The other phases of vanadium oxide ( $\text{VO}$ ,  $\text{VO}_2$ ,  $\text{V}_2\text{O}_3$ ) have multiple crystal phases, but  $\text{V}_2\text{O}_5$  exists only as an orthorhombic crystal (Figure 1.3) which is fundamentally comprising of  $\text{VO}_5$  pyramids that form alternating double chains along the b-axis (Walia et al., 2013). Hence,  $\text{V}_2\text{O}_5$  has a strong tendency for the crystallites in a powder or a texture to be oriented or grew in belt shapes (Sharma et al., 2015).

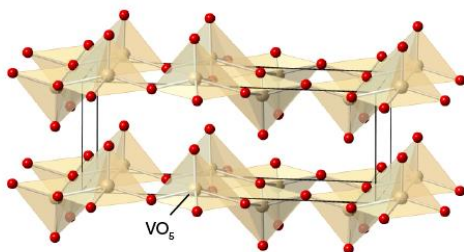


**Figure 1.2: Orthorhombic crystal system of  $\text{V}_2\text{O}_5$ .**  
(<http://www.chemtube3d.com/solidstate/SS-V2O5.htm>)

Among the oxides of vanadium,  $\text{V}_2\text{O}_5$  melted at  $690^\circ\text{C}$  (MSDS, n.d.), an orange-red powder and partially soluble in water to give a pale yellow acidic solution, and which dissolves readily in alkalis to form vanadates. Meanwhile, it is also soluble in strong acids.  $\text{V}_2\text{O}_5$  is widely used in analytical chemistry due to the  $\text{V}_2\text{O}_5$  ion can form slightly soluble or intensely colored, simple or complex compounds with inorganic and organic substances (Manskaya et al., 1968).

$\text{V}_2\text{O}_5$  is widely used in thin-films device application due to its phase transition behavior. When the vanadium oxide thin film was heated to a specific temperature, it will present a phase transition indicated by the changes of its electrical and optical properties (Ya et al., 2014). An insulating thin film with good dielectric properties also has wide range of applications in various electronic devices, hence the dielectric properties of  $\text{V}_2\text{O}_5$  thin film has drawn much attention from researchers (Thomas et al., 1989).

### 1.3 Conventional Solid State Method

Conventional solid state method is widely used to prepare polycrystalline solid from mixture of starting materials. Furthermore, this method is low cost and high yield which is another advantage to become a preference of many researchers. In recent years, the materials synthesis and processing become crucial for materials development. As a result, the importance of sintering increases as materials processing technology.

The purpose of the sintering process is to produce sintered parts with reproducible and designed microstructure through controlling the sintering variables. Microstructure control means the control of grain size, sintered density, size and distribution of other

phases including pores. Sintering processes can be categorized into two types: solid state sintering and liquid phase sintering. Solid state sintering occurred when the powder pelletized or densified completely in a solid state at the sintering temperature. At higher sintering temperatures, liquid phase sintering occurs in the powder compact during sintering.

The sinterability and sintered microstructure of a powder compact were determined by several variables. They may divide into two categories: materials variables and process variables. The materials variables include chemical composition of powder compact, size, shape, size distribution, etc. These variables influence densification and grain growth. The homogeneity of the powder mixture also takes a significant role. The other variables related to sintering condition (process variables) are mostly thermodynamic variables, such as temperature, time, pressure, atmosphere, heating and cooling rate, etc (Randall, 1996).

#### **1.4 Mechanical Alloying Method**

Mechanical alloying is a dry, solid state powder, high-energy ball milling technique. This technique has been widely used to produce a variety of commercially usages and scientific purposes.

Usually we can easily found two terms used in the literature to denote the processing of powder particles in high-energy ball mills. Mechanical Alloying (MA) describes the process when mixtures of powders (metals or alloy) are milled together. However, the milling of uniform composition powders, such as pure metals, intermetallics, or prealloyed powders for a reduction in particle size, but not for the materials homogeneities, has been named as Mechanical Milling (MM) (Suryanarayana, 2001).

MA is a well-known high-energy ball milling method for materials in powder form which requires neither high temperature or heating nor using expensive equipment (Loginov et al., 2015). The powders are trapped between the grinding balls in a vial during milling. The powder particles undergo repeated severe plastic deformation and fracture processes, resulting incorporation of lattice defects and to a continuous refinement to the nanocrystalline size. On the other hand, the milling conditions also played important roles in the milling process. For instance, the mechanical behavior of the powder components such as, their phase equilibria, and the stress state during milling can then result in intermixing, solid state interdiffusion and supersaturation beyond the equilibrium solubility limit and chemical reaction, lastly resulting in metastable phase formation (Suryanarayana, 2001; Eckert et al., 1991; Raanaei et al., 2015; Scudino et al., 2009).

This method carried out by using SPEX SamplePrep 8000D Mixer/Mill (Figure 4.1), are able to mill about 8-20 g of the powder at a time depending on the size of the vials (Figure 4.2). The grinding balls move energetically back and forth for several thousand times a minute, thus crushing and milling the powders and consequently, a homogeneous mixed

composites with smaller particle size powders was obtained (Loginov et al., 2015; Azimi et al., 2014).

### **1.5 Objective**

1. To prepare and characterize mixed oxides 60 mol% of  $2\text{MnO}_2$  and 40 mol%  $\text{V}_2\text{O}_5$  by conventional solid state reaction method and mechanical alloying method at different sintering temperatures,  $500^\circ\text{C}$  -  $800^\circ\text{C}$ .
2. To study the morphology and phase composition changes of the samples at different sintering temperatures.
3. To study the electrical and thermal properties of different Mn-V oxides phases under different measuring temperatures,  $30^\circ\text{C}$  -  $400^\circ\text{C}$ .

### **1.6 Hypothesis**

1. The average grain size would increase with sintering temperature.
2. Phase composition of starting materials would decrease while phase composition of Mn-V oxides would increase with sintering temperature.
3. Electrical conductivity, dielectric constant and dielectric loss factor of the samples would increase as measuring temperature increases. And, thermal diffusivity would decrease with increase in measuring temperature.

### **1.7 Outlines of the Present Study**

The present thesis consists of 6 chapters. First of all, Chapter 1 briefly presents the background and the importance of the project followed by the introduction of the preparation techniques used in this project which are conventional solid state method and mechanical alloying method. The introduction of the starting materials manganese oxide and vanadium oxide are also included, followed by the objectives of this research. Chapter 2 deals with the previous published works which are related to the present study. Chapter 3 discussed the mechanism regarding sample preparation methods, theory and basic principles related to this study. Chapter 4 mainly describes the experimental methodology for the preparation of the mixed oxide of Mn and V which are conventional solid state and mechanical alloying methods. From the flow charts, the procedures of sample preparation are completely presented with detail description of each procedure using two methods followed by the details of dielectric measurement and characterization techniques. Chapter 5 presents the discussion toward the results obtained, comparison between the samples at different sintering temperatures, measuring temperatures and frequencies. Lastly, Chapter 6 summarizes all the results and presented significant results and conclusion. Some recommendations for future work related to this research are also suggested.



## BIBLIOGRAPHY

- Afifi M., Bekheet A., Elwahhab E. A. and Atyia H., (2001). Ac conductivity and dielectric properties of amorphous  $\text{In}_2\text{Se}_3$  films from *Vacuum* 61: 9-17.
- Ahmadu U., Tomas S., Jonah S., Musa A. and Rabiun N., (2013). Equivalent circuit models and analysis of impedance spectra of solid electrolyte  $\text{Na}_{0.25}\text{Li}_{0.75}\text{Zr}_2(\text{PO}_4)_3$  from *Advance Material Letters* 4 (3): 185-195.
- Ahmed R., Moslehuddin A., Mahmood Z. H. and Akther Hossain A. (2015). Weak ferromagnetism and temperature dependent dielectric properties of  $\text{Zn}_{0.9}\text{Ni}_{0.1}\text{O}$  diluted magnetic semiconductor from *Materials Research Bulletin* 63: 32-40.
- Alex S., Jumiah H., Mansor H. and Zaidan A. W. (2014). Thermal diffusivity of kaolinite-mullite ceramic matrix composite with silicon nitride nanoparticle with silicon nitride nanoparticles filler from *Thermochimica Acta* 593: e76-e81.
- Ali M., Khan M., Chowdhury F., Akhter S. and Uddin M. (2015). Structural properties, impedance spectroscopy and dielectric spin relaxation of Ni-Zn ferrite synthesized by double sintering technique, [electronic version]. Retrieved 1<sup>st</sup> Jan 2016 from <http://arxiv.org/ftp/arxiv/papers/1505/1505.06438.pdf> .
- Almond D. (1983). Mobile ion concentrations in solid electrolytes from an analysis of AC conductivity from *Solid State Ionic* 9 & 10: 277-282.
- Amelo B., (2012). X'Pert HighScore Plus, version 3.0e, The Netherland.
- Anantha P. and Hariharan K. (2005). ac Conductivity analysis and dielectric relaxation behaviour of  $\text{NaNO}_3\text{-Al}_2\text{O}_3$  composites from *Materials Science and Engineering B* 121: 12-19.
- Anderson O. and Stuart D. (1954). Calculation of activation energy of ionic conductivity in silica glasses by classical methods from *Journal of American Ceramic Society* 37: 573.
- Anthony J. W., Bideaux R. A., Bladh K. W. and Nichols M. C. (1990). *Handbook of Mineral*, Chantilly, VA.: Mineral Data Publishing.
- Arpaci V. S., Shu-Hsin K. and Selamet A. (1999) *Introduction to heat transfer*, Upper Saddle River, NJ.: Prentice-Hall, Inc..
- Attia A., Soliman H., Saadeldin M. and Sawaby K. (2015). AC electrical conductivity and dielectric studies of bulk p-quaterphenyl from *Synthetic Metals* 205: 139-144.
- Awad M., Ahmed A., Khavrus V. and Ibrahim E. (2015). Tuning the morphology of ZnO nanostructure by doping and the associated variation in electrical and optical properties from *Ceramic International* 41: 10116-10124.
- Azimi A., Shokuhfar A. and Zolriasatein A. (2014). Nanostructure Al-Zn-Mg-Cu-Zr alloy prepared by mechanical alloying followed by hot pressing from *Material Science & Engineering A* 595:124-130.

- Bajpai P. and Singh K. (2011). Dielectric relaxation and ac conductivity study of  $\text{Ba}(\text{Sr}_{1/3}\text{Nb}_{2/3})\text{O}_3$  from *Physica B* 406: 1226-1232.
- Bakonyi I., Toth-Kadar E., Tarnoczi T., Varga L., Cziraki A., Gerocs I. and Fogarassy B. (1993). Structure and properties of fine-grained electrodeposited nickel from *NanoStructure and Materials* 3: 155-161.
- Bang L., S. Ming, Lin T., C. Gao, Lin Y., Shaomin P. and Jie X., (). "Ultra-long  $\alpha$ - $\text{MnO}_2$  nanowires: Control synthesis and its absorption activity," *Materials Letters*, vol. 121, pp. 234-237, 2014.
- Barsoukov B. and Macdonald J. R., *Impedance Spectroscopy- Theory, Experiment, and Applications. Second Edition*, New Jersey: John Wiley.
- Bekheet A. and Hegab N. (2009). Ac conductivity and dielectric properties of  $\text{Ge}_{20}\text{Se}_{75}\text{In}_5$  films from *Vacuum* 83: 391-396.
- Benjamin J. and Volin T. (1974). The Mechanism of Mechanical Alloying from *Metallurgical Transactions* 5: 1929-1934.
- Bhaskaran, Sriram S., Strano M. S. and Kalantar-zadeh K. (2013). Transition metal oxides-Thermoelectric properties from *Progress in Material Science* 58: 1443-1489.
- Bin W., Jianjiun L., Hui L., Haoming H. and Sihai C. (2013). Nanosturcutred vanadium oxide thin film with high TCR at room temperature for microbolometer from *Infrared Physics & Technology* 57: 8-13.
- Blythe T. and Bloor D. (2005). *Electrical Properties of Polymers, Second Edition*, New York: Cambridge University Press.
- Bordeneuve H., Guillemet-Fritsch S. and Rousset A. (2009). Structure and electrical properties of single-phase cobalt manganese oxide spinels  $\text{Mn}_{3-x}\text{Co}_x\text{O}_4$  sintered classically and by spark plasma sintering (SPS) from *Solid state chemistry* 182: 396-401.
- Buraidah M., Teo L., Majid S. and Arof A. (2009). Ionic conductivity by correlated barrier hopping in  $\text{NH}_4\text{I}$  doped chitosan solid electrolyte from *Physica B* 404: 1373-1379.
- Chambers R. (1990). *Electrons in Metals and Semiconductors*, Great Britain: St Edmundsbury Press.
- Chen L., Ong C., Neo C., Varadan V. and Varadan V., (2004). *Microwave Electronics, measurement and material characterisation*, West Sussex: John Wiley & Sons Ltd.
- Cheng-Shong H., Sheng-Yuan C., Cheng-Che T. and Wen-Chang S. (2011). Manganese effect on the relaxation behaviors of the space charge polarization in  $\text{Pb}(\text{Fe}_{2/3}\text{W}_{1/3})_{0.9}\text{Ti}_{0.1}\text{O}_3$  ceramics from *Ceramics International* 37: 3405-3411.

- Chi Kao K. (2004). *Dielectric Phenomena in Solid*, California: Elsevier Academic Press.
- Chun Yan L., Jumiah H., Mansor H., Swee Yin W., Foo Khoon T. and Yick Jeng W., (2011). Effect of Sintering Temperature on the Microstructure and Dielectric Properties of SrTiO<sub>3</sub> from *World Applied Science Journal* 14(7): 1091-1094.
- Cowley R., (1980). Structural phase transitions I. Landau theory from *Advances in physics* 29: 1-110.
- Dakhel A. (2006). Correlated structural and electrical properties of thin manganese oxide films from *Thin Solid Films* 496: 353-359.
- Deger D., Ulutas K., Yakut S. and Kara H. (2015) Dielectric properties and ac conductivity of TlSbTe<sub>2</sub> thin films from *Material Science in Semiconductor Processing* 38: 1-7.
- Di Blasi O., Briguglio N., Busacca C., Ferraro M., Antonucci V. and Di Blasi A. (2015). Electrochemical investigation of thermally treated graphene oxides as electrode materials for vanadium redox flow battery from *Applied Energy* 147: 74-81.
- Dongfang Y., (2013). Pulsed laser deposition of vanadium-doped manganese oxide thin films for supercapacitor applications from *Journal of Power Sources* 228: 89-96.
- Eckert J. and Schultz L. (1991). Amorphization reaction during mechanical alloying: influence of the milling conditions from *Journal of Materials Science* 26: 441-446.
- Fau P., Bonino J. and Rousset A. (1994). Electrical properties of sputtered MnO<sub>2</sub> thin films from *Applied Surface Science* 78: 203-210.
- Fernandez J., Caballero A., Villegas M., Khatib S., Banares M., Fierro J., Costa-Kramer J., Lopez-Ponce E., Martin-Gonzalez M., Briones F., Quesada A., Garcia M. and Hernando A. (2006). Structure and magnetism in the Zn-Mn-O system: A candidate for room temperature ferromagnetic semiconductor from *Journal of the European Ceramic Society* 26: 3017-3025.
- Fernandez-Palacios S., Santos-Gomez L., Compana J., Porras-Vazpuez J., Cabeza A., Marrero-Lopez D. and Losilla E. (2015). Influence of the synthesis method on the structure and electrical properties of Sr<sub>1-x</sub>K<sub>x</sub>GeO<sub>3-x</sub> from *Ceramics International* 41: 6542-6551.
- G. Will, (2006). *Powder Diffraction: The Rietveld Method and the Two-Stage Method*, Bonn, Germany: Springer,
- Gao W. and Sammes N. M., (1999). *An Introduction to Electronic and Ionic Materials*, Singapore: World Scientific.
- Gerhardt R. (1994). Impedance and dielectric spectroscopy revisited: Distinguishing localized relaxation from long-range conductivity from *J. Physics Chemistry Solids* 55: 1491-1506.

- Godse A. and Bakshi U. (2009) *Basic electronics, Volume 1*, Pune, India: Technical Publication Pune.
- Gouda G. M. and Nagendra C. (2009). Structural and electrical properties of mixed oxides of manganese and vanadium: A new semiconductor oxide thermistor material from *Sensors and Actuators A* 155: 263-271.
- Gouda G. M. and Nagendra C. (2013) Preparation and characterization of thin film thermistors of metal oxides of manganese and vanadium (Mn-V-O) from *Sensors and Actuators A* 190: 181-190.
- Hirschorn B., Orazem M. E., Tribollet B., Vivier V., Frateur I. and Musiani M. (2010). Determination of effective capacitance and film thickness from constant-phase-element parameters from *Electrochimica Acta* 55: 6218-6227.
- Hodge I., Ingram M. and West A. (1976). Impedance and modulus spectroscopy of polycrystalline solid electrolytes from *J. Electroanal Chem.* 74: 125-143.
- Hongtao G., Gang C., Jing Z. and Yude W. (2010). Temperature dependent dielectric characterization of manganese dioxide nanostructures with different morphologies at low frequency from *Journal of Alloys and Compounds* 507: 126-132.
- Hongtao G., Yude W., Gang C. and Jing Z. (2012). Frequency and temperature effects on dielectric and electrical characteristics of  $\alpha\text{MnO}_2$  nanorods from *Powder Technology* 224: 356-359.
- Howell B., JR and Licastro P. (1961). Dielectric behavior of rock and minerals from *The American Mineralogist* 46: 269-288.
- Hsing-I H., Chi-Shiung H., Chi-Yao T. and Li-Then M. (2015). Cobalt-substitution effect on dielectric properties of CuZn ferrites from *Ceramics International* 41: 4140-4144.
- Hussain M., Nadeem M., Hongyu S., Shafqat S., Nisar A., Khan M. and Ahmad M. (2015). Electrical transport properties of single crystal vanadium pentoxide nanowires from *Material Chemistry and Physics* 159: 10-24.
- HyperPhysics. N.d. Retrieved 5 May 2015 from <http://hyperphysics.phy-astr.gsu.edu/hbase/pertab/tranel.html>.
- Inorganic Crystal Structure Database ICSD v2014-01, FIZ Karlsruhe and the National Institute of Standards and Technology (NIST): N.p. 2014.
- Jianjun L., Chun-Gang D., Wei-Guo Y., Mei W., Smith R. and Hardy J. (2003). Dielectric permittivity and electric modulus in  $\text{Bi}_2\text{Ti}_4\text{O}_{11}$  from *Journal of Chemical Physics* 119: 2812-2819.
- Jiaping H., Mingrong S. and Wenwu C. (2002). Hopping conduction in Mn-doped ZnO from *Applied physics letters* 82: 67-69.

- Ji-Won L. and Jung-Hyuk K. (2015). Grain size effects on the dielectric properties of  $\text{CaCu}_3\text{Ti}_4\text{O}_{12}$  ceramics for supercapacitor applications from *Ceramics International* 41: 10442-10447.
- Junhua J. and Kucernak A. (2002). Electrochemical supercapacitor material based on manganese oxide: preparation and characterization from *Electrochimica Acta* 47: 2381-2386.
- Kayan A., Tarcan E., Kadiroglu U. and Esmer K. (2004). Electrical and dielectrical properties of the  $\text{MnO}_2$  doped with  $\text{As}_2\text{O}_3$  and  $\text{SnO}$  from *Material Letters* 58: 2170-2174.
- Kemmitt R. and Peacock R. (1975). *The Chemistry of MANGANESE, TECHNETIUM and RHENIUM*, Britain: Pergamon Texts in Inorganic Chemistry Volume 13.
- Kocks U., Tome C. and Wenk H. (1998). *Texture and Anisotropy*, New York: Cambridge University Press.
- Kumar A. and Kumar A. (2004). Dependence of activation energy and pre-exponential factor on electric field in bulk  $\text{Se}_{90}\text{Sb}_{10-x}\text{Ag}_x$  glassy alloys from *Journal of Non-Crystalline Solid* 386: 51-55.
- Kumar A., Dwivedi R. and Pal V. (2012). Dielectric Behavior and Impedance Spectroscopy of  $\text{Ba}_{1-x}\text{Bi}_x\text{Ti}_{1-x}\text{Fe}_x\text{O}_3$  from *Advanced Materials Research* 585: 190-194.
- Lakhdar M., Larbi T., Ouni B. and Amlouk M. (2015). AC conductivity, dielectric relaxation and modulus behavior of  $\text{Sb}_2\text{S}_3$  new kermesite alloy for optoelectronic applications from *Material science in semiconductor processing* 40: 596-601.
- Lee J. H., Kim Y. H., Ahn S. J., Ha T. H. and Kim H. S. (2015) Grain-size effect on the electrical properties of nanocrystalline indium tin oxide thin films from *Material Science and Engineering B* 199: 37-41.
- Lei S., Tang K. and Chen C. (2007). Preparation of aligned  $\text{MnV}_2\text{O}_6$  nanorods and their anodic performance for lithium secondary battery use from *Nanotechnology* 18: 1-7.
- Liu P., Qing H., Hou H., Wang Y. and Zhang Y. (2016). EMI shielding and thermal conductivity of a high porosity reticular titanium foam from *Materials and Design* 92: 823-828.
- Loginov P., Levashov E., Kurbatkina V., Zaitsev A. and Sidorenko D. (2015). Evolution of the microstructure of Cu-Fe-Co-Ni powder mixtures upon mechanical alloying from *Powder Technology* 276: 166-174.
- Lu L. and Lai M. (1995). Formation of new materials in the solid state by mechanical alloying from *Materials & Design* 16: 33-39.
- Macdonald J. R. and Kenan W. R. (1987) *Impedance Spectroscopy*, New York: John Wiley & Sons.

- Mandouh Z. El and Selim M. (2000). Physical Properties of vanadium pentoxide sol gel films from *Thin Solid Films* 371: 259-263.
- Mansfield M. and O'Sullivan C., (2011). *Understanding Physics*, United Kingdom: Joh Wiley & Sons.
- Manskaya S. and Drozdova T. (1968). *Geochemistry of Organic Substances*, Hungary: International Series of Monographs in Earth Science.
- MSDS of MnO<sub>2</sub>, n.d. Retrieved 5<sup>th</sup> of June 2015 from <http://www.espimetals.com/index.php/msds/665-manganese-oxide-mno2>.
- MSDS of V<sub>2</sub>O<sub>5</sub>, n.d. Retrieved 5<sup>th</sup> of June 2015 from <http://www.strem.com/downloads/MSDS/93-2321.pdf>
- Matula R. (1979). Electrical Resistivity of Copper, Gold, Palladium and Silver from *J. Phys. Chem. Ref. Data* 8(4): 1147-1298.
- Mocala K. and Ziolkowski J., (1987). Polymorphism of the bivalent metal vanadates MeV<sub>2</sub>O<sub>6</sub> (Me=Mg, Ca, Mn, Co, Ni, Cu, Zn, Cd) from *Journal of solid state chemistry* 69: 299-311.
- Mohakud P. S. (2009). *Structrures and properties of Al-Based Al-Si-Ni nanostructures developed by mechanical alloying*, Master Thesis, National Institute of Technology, Rourkela.
- Molenda J., Stoklosa A. and Znamirovski W. (1987). Electrical properties of manganese doped ferrous oxide at high temperature from *Solid State Ionics* 24: 39-44.
- Morishita T., Nomura K., Inamasu T. and Inagaki M. (2005). Synthesis of anhydrous manganese vanadate powder by coprecipitation and its anodic performance for lithium secondary battery from *Solid State Ionic* 176: 2235-2241.
- Neagu A. M., Ciuchi I. V., Curecheriu P. and Mitoseriu L. (2010). Impedance spectroscopy characterization of collagen samples from *Journal of Advanced Research in Physics* 1: 1-4.
- Okutan M., Basaran E., Bakan H. I. and Yakuphanoglu F. (2015). AC conductivity and dielectric properties of Co-doped TiO<sub>2</sub> from *Physica B* 364: 300-305.
- Orazaem M. E., Shukla P. and Membrino M. A. (2002). Extension of the measurement model approach for deconvolution of underlying distribution for impedance measurements from *Electrochimica Acta* 47: 2027-2034.
- Park H.K. (2005). Manganese vanadium oxides as cathodes for lithium batteries from *Solid State Ionics* 176: 307-312.
- Popovic Z. and Popovic B. D. (2000). *Introductory Electromagnetics*, New Jersey: Prentice-Hall.

- Preisler E. (1976). Semiconductor properties of manganese dioxide from *Journal of applied electrochemistry* 6: 311-320.
- Privitera S., Mio A., D'Arrigo G., Carria E. and Rimini E. (2013). Proceedings from E\PCOS 2013: *Effects of the amorphous structure on the electrical conductivity and the crystallization kinetics of GeTe thin films*. European Phase Change and Ovonic Symposium: Berlin, Germany,.
- Raanaei H., Abbasi S. and Behaein S. (2015). Structural and magnetic evolution of nanostructured  $\text{Co}_{40}\text{Fe}_{10}\text{Zr}_{10}\text{B}_{40}$  prepared by mechanical alloying from *Journal of Magnetism and Magnetic Materials* 384: 175-180.
- Rahaman M., (2003). *Ceramic Processing and Sintering, Second Edition*, USA: CRC Press.
- Rajput R. (2003). *Electrical Engineering Materials*, New Delhi: Laxmi Publication (P) Ltd.
- Raju G. G. (2003). *Dielectrics in Electric Fields*, New York: Marcel Dekker, Inc..
- Ramana C., Hussain O., Naidu B. S., Julien C. and Balkanski M. (1998). Physical investigation on electron-beam evaporated vanadium pentoxide films from *Material Science and Engineering B52*: 32-39.
- Randall M. (1996). *Sintering theory and practice*. United State:Wiley-interscience.
- Ranjith K. E. and Jayaprakash R. (2014). The role of fuel concentration on particle size and dielectric properties of manganese substituted zinc ferrite nanoparticles from *Journal of Magnetism and Magnetic Materials* 366: 33-39.
- Rao V. L., Shekharam T., Kumar T. and Nagabhushanam M. (2015). Effect of copper on impedance and dielectric studies of  $\text{Cu}_x\text{Zn}_{1-x}\text{S}$  mixed semiconductor compounds from *Material Chemistry and Physics* 159: 83-92.
- Rodgers R. S., Research Solution and Resources. 1999. Retrieved 29<sup>th</sup> June 2015 from <http://www.consultrsr.net/index.htm>.
- Ropp R. (2003). *Solid State Chemistry*, The Netherlands: Elsevier Science B.V.
- Satyanarayana N., 2010. *Synthesis, characterization and transport studies of lithium based superionic conductors for solid state battery applications*, PhD Thesis, Pondicherry University, India.
- Schmidt R., Basu A., Brinkman A., Klusek Z. and Datta P. (2005). Electron-hopping modes in  $\text{NiMn}_2\text{O}_4+\delta$  materials from *Applied Physics Letter* 86: 073501.
- Scudino S., Sakaliyska M., Surreddi K. and Eckert J. (2009). Mechanical alloying and milling of Al-Mg alloys from *Journal of Alloys and Compounds* 43: 2-7.
- Sears F. W., Zemansky M. W. and Young H. D. (1984). *University Physics, sixth edition*, USA: Addison-Wesley Series in Physics.

- Sharma R. K., Kumar P. and Reddy G. (2015). Synthesis of vanadium pentoxide ( $V_2O_5$ ) nanobelts with high coverage using plasma assisted PVD approach from *Journal of Alloys and Compounds* 638: 289-297.
- Shklovskii B. and Efros A. (1984). *Electronic properties of doped semiconductors*, New York: Springer.
- Shvalya V., Oleaga A., Salazar A., Kohutych A. and Vysochanskii Y. (2015). Critical behaviour study of ferroelectric semiconductors  $(Pb_xSn_{1-x})_2P_2S_6$  from thermal diffusivity measurements from *Thermochimica Acta* 617: 136-143.
- Sinclair D. and West A. (1989). Impedance and modulus spectroscopy of semiconducting  $BaTiO_3$  showing positive temperature coefficient of resistance from *Journal of Applied Physics* 66(8): 3850.
- Singh M., Hlabana K. K., Singhal S. and Devlal K., (2015). Grain-size effect on the thermal conductivity of nanosolids from *Journal of Taibah University for Science* XXX: XXX-XXX.
- Snelling E. (1988) *Soft Ferrites: Properties and Applications*, UK: Butterworth-Heinemann.
- Snellings R., Machiels L., Mertens G. and Elsen J. (2010). Rietveld refinement strategy for quantitative phase analysis of partially amorphous zeolitized tuffaceous rocks from *Geologica Belgica* 13 ( 3): 183-196.
- Solymar L. and Walsh D. (1979). *Lectures on the electrical properties of materials*, Great Britain: Oxford University Press.
- Subramanian M., (1992). High pressure synthesis of pyrochlore-type manganese vanadate and related compositions from *Materials Research Bulletin* 27: 939-943.
- Suryanarayana C. (1999). *Non-equilibrium Processing of Materials*, UK: Elsevier Science.
- Suryanarayana C. (2001). Mechanical alloying and milling from *Progress in Material Science* 46: 1-184.
- Thomas B. and Jayalekshmi S. (1989). "Dielectric properties of vanadium pentoxide thin films in the audiofrequency range from *Journal of Non-Crystalline Solides* 113:65-72.
- Thompson C. V. (1990) Grain Growth in Thin Films from *Annu. Rev. Mater. Sci.* 20: 245-268.
- Tong T. (1994) *Thermal Conductivity* 22, Pennsylvania, USA: Technomic Publishing Company.
- Tsuda N., Nasu K., Yanase A. and Siratori K. (1991). *Electronic Conduction in Oxides*, Germany: Springer-Verlag Berlin Heideberg.



- Tzou D., (2015) *Macro- to microscale heat transfer The lagging behavior*, West Sussex, United Kingdom: John Wiley & Sons, Ltd..
- Tzu Hsuan C. and Tso-Ming C. (2015). Synthesis and characterization of single-crystalline vanadium pentoxide by the low-temperature of glycothermal method from *Materials Letter* 157: 205-208.
- Vemuri R., Bharathi K., Gullapalli S. and Ramana C. (2010). Effect of structure and size on the electrical properties of nanocrystalline WO<sub>3</sub> Films from *Applied Materials & Interfaces* 2: 2623-2628.
- Vilar S. Y., Castro-Couceiro A., Rivas-Murias B., Fondado A., Mira J., Rivas J. and Senaris M., (2005). High Dielectric Constant in the charge-ordered manganese oxide CaMn<sub>7</sub>O<sub>12</sub> from *Z. Nnorg. Allg. Chem.* 631: 2192-2196.
- Walia S., Balendhran S., Nili H., Zhuiykov S., Rosengarten G., Hua Wang Q., Bhaskaran M., Sriram S., Strano. M.S., Kalantar-zadeh K. (2013). Transition metal oxides- Thermoelectric properties from *Progress in Material Science* 58: 1443-1489.
- Wang Q., Wang Q. and Wan C. (2010). Effect of Sintering Time on the Microstructure and Properties of Inorganic Polyphosphate Bioceramics from *Science of Sintering* 42: 337-343.
- WenLiang H., YongCai Z., XiaoXue Z., Hao W. and Hui Y. (2003). Low temperature preparation of nanocrystalline Mn<sub>2</sub>O<sub>3</sub> via ethanol-thermal reduction of MnO<sub>2</sub> from *Journal of Crystal Growth* 252: 285-288.
- West A. R. (1987). *Solid State Chemistry and its Applications*, UK: Wiley.
- Will G. (2006) *Powder Diffraction: The Rietveld Method and the Two-Stage Method*, Bonn, Germany: Springer.
- Xiaochun W., Fachun L., Limei L., Yongzeng L., Lianghui L., Yan Q. and Zhigao H., (2008). Influence of thermal cycling on structural, optical and electrical properties of vanadium oxide thin films from *Applied Surface Science* 255: 2840-2844.
- X'Pert HighScore Plus, version 3.0e* (2012) Amelo B.: The Netherlands.
- Ya Q., Jie C., Yuan L., Xing Y., Hua Y. and Kai X., (2014). Fabrication of low phase transition temperature vanadium oxide films by direct current reactive magnetron sputtering and oxidation post-anneal method from *Infrared Physics & Technology* 67: 126-130.
- Yakuphanoglu F., Evin E. and Okutan M. (2006). The dielectrical and alternating current conductivity properties of 40Cu+20Co+40Y<sub>2</sub>O<sub>3</sub> ceramic from *Physica B* 382: 285-289.
- Yakuphanoglu F., Zaitsev D., Trusov L. and Kazin P. (2007) Electrical conductivity and electrical modulus properties of 13SrO-5.5Fe<sub>2</sub>O<sub>3</sub>-0.5Al<sub>2</sub>O<sub>3</sub>-8B<sub>2</sub>O<sub>3</sub> magnetic glass ceramic from *Journal of Magnetism and magnetic materials* 312: 43-47.

- Yaru W., Yongping P. and Panpan Z. (2015). Investigation of dielectric relaxation in BaTiO<sub>3</sub> ceramics modified with BiYO<sub>3</sub> by impedance spectroscopy from *Journal of alloy and compounds* 653: 596-603.
- Young H. D. and Freeman R. A. (2008) *University Physics, 12th Edition*, San Francisco: Pearson Addison-Wesley.
- Yude W., Hongtao G., Gang C. and Shubo Z. (2010). Microwave absorption characteristics of manganese dioxide with different crystalline phase and nanostructures from *Material Chemistry and Physics* 124: 639-645.
- Zabriky J. (2009). *The chemistry of metal enolates*, London: A John Wiley and sons.
- Zhang N., Li Q., Huang S., Yu Y., Zheng J., Cheng C. and Wang C. (2015). Dielectric relaxation in multiferroic La<sub>2</sub>Ti<sub>2</sub>O<sub>7</sub> ceramic from *Journal of alloys and compounds* 652: 1-8.
- Zhangli H., Changhong C., Chaohong L. and Sihai C. (2013). Tungsten-doped vanadium dioxide thin films on borosilicate glass for smart window application from *Journal of alloys and compounds* 564: 158-161.
- Zhong Jie Z., Liang Xiao C. and Xiang Ying C. (2015). Nitrogen/manganese oxides co-doped nanoporous carbon materials: Structure characterization and electrochemical performances for supercapacitor applications from *Electrochimica Acta* 161: 84-94.